BSM Higgs Searches in Tau Final States at DØ

L. Suter([1])

([1]) *The University of Manchester - Manchester, UK.*

Summary. — We present a search for beyond the standard model (BSM) Higgs bosons in τ lepton final states at DØ. Data were collected by the DØ detector in proton-antiproton collisions at a center-of-mass energy of $\sqrt{s} = 1.96$ TeV during Run II at the Tevatron with up to 7.0 fb^{-1} of integrated luminosity. The results are used to set 95% C.L. limits on the pair production cross section on these BSM Higgs bosons.

PACS 1 – 4.80 Fd
PACS 1 – 3.85 Rm

1. – Introduction

Beyond the standard model (BSM) Higgs boson searches in τ final states are of specific interest as several BSM theories, such as Supersymmetry, predict enhanced couplings to τ leptons. Supersymmetry (SUSY) is an extension to the standard model (SM) that predicts an additional symmetry between bosons and fermions. SUSY has several advantages over the SM, such as the introduction of a dark matter candidate, a solution to the hierarchy problem and a potential for GUT scale unification. The minimal supersymmetric standard model, MSSM, [1] is the simplest version of a SUSY theory. It predicts, after symmetry breaking, five Higgs bosons of which three are neutral and two charged, denoted by h, H, A, H^+ and H^-. In the MSSM the coupling of the neutral Higgs to down-type quarks and leptons is enhanced by a factor of $\tan\beta$ and the corresponding coupling to the up-type quarks and leptons is suppressed. This means that decay modes to bottom quarks and tau leptons are dominant with a predicted decay rate of around 90% to bottom quarks and 10% to tau leptons. At a hadron collider, the bottom quark channel is background dominated from multijet production.

In other BSM theories, Higgs bosons with higher multiplicities of charge can be created. In Higgs triplet models, for example, Higgs bosons with a double charge, $H^{\pm\pm}$, can be produced. For these doubly-charged Higgs bosons various models predict the decay of the $H^{\pm\pm}$ to τ leptons to be of specific importance. The 3-3-1 model of Ref. [2] predicts that the decays $H^{\pm\pm} \to \tau^{\pm}\tau^{\pm}$ are dominant. Assuming the normal hierarchy of neutrino masses in a seesaw neutrino mass mechanism leads to approximately equal

branching fractions for $H^{\pm\pm}$ boson decays to $\tau\tau$, $\mu\tau$, and $\mu\mu$, if the mass of the lightest neutrino is less than 10 meV [3].

Left-right symmetric models can be considered to be a general Higgs triplet model. These predict both right-handed ($H_R^{\pm\pm}$) and left-handed states ($H_L^{\pm\pm}$). These are characterized through their coupling to right and left-handed fermions, respectively. The cross section for production of right-handed $H_R^{++}H_R^{--}$ pairs is about a factor of two smaller than for $H_L^{++}H_L^{--}$ because of the different coupling to the Z boson [4]. The mass limits for $H_R^{\pm\pm}$ bosons therefore tend to be weaker than for $H_L^{\pm\pm}$ bosons.

In these proceedings I summarize the first search for $H^{\pm\pm} \to \tau^{\pm}\tau^{\pm}$ decays at a hadron collider. This analysis is based on data collected with the DØ detector at the Fermilab Tevatron Collider which corresponds to an integrated luminosity of up to 7.0 fb^{-1} [5]. The decay of the $H^{\pm\pm}$ into tau leptons and muons was studied. Limits were set for left-handed and right-handed Higgs for three model independent cases, when $\mathcal{B}(H_L^{\pm\pm} \to \tau^{\pm}\tau^{\pm}) = 1$, $\mathcal{B}(H_L^{\pm\pm} \to \mu^{\pm}\tau^{\pm}) = 1$ and when the $\mathcal{B}(H_L^{\pm\pm} \to \tau^{\pm}\tau^{\pm}) + \mathcal{B}(H_L^{\pm\pm} \to \mu^{\pm}\tau^{\pm}) = 1$. Limits were in addition set for a left-handed Higgs for one model dependent case, with equal branching ratios to $\tau\tau$, $\mu\mu$ and $\tau\mu$ states as predicted by [3].

2. – The Doubly Charged Higgs

The analysis summarized here assumes that $H^{\pm\pm}$ Higgs bosons could be pair-produced through the mechanism $q\bar{q} \to Z/\gamma^* \to H^{++}H^{--} \to \ell^+\ell'^+\ell^-\ell'^-$ ($\ell, \ell' = e, \mu, \tau$), where the $H^{\pm\pm}$ decays to τ and μ leptons. Single production of $H^{\pm\pm}$ bosons through W exchange, leading to $H^{\pm\pm}H^{\mp}$ final states, is not considered in the analysis presented here to reduce the model dependency of the results [6]. The decay of $H^{\pm\pm}$ into electrons is also not considered [5]. This analysis also considers decays to mixed flavor lepton pairs, since all $H^{\pm\pm}$ decays violate lepton flavor number conservation.

The $H^{\pm\pm}$ bosons have been searched for previously at the LEP e^+e^- Collider at CERN [7] and at the HERA ep Collider at DESY [8]. Limits were set on the mass of the $H^{\pm\pm}$ boson between $95 - 100$ GeV, for τ leptons, muons and electrons. Single $H^{\pm\pm}$ production was studied by the OPAL and H1 Collaborations in the processes $e^+e^- \to e^{\mp}e^{\mp}H^{\pm\pm}$ [9] and $e^{\pm}p \to \ell^{\mp}H^{\pm\pm}p$ [8]. In addition, OPAL also studied Bhabha scattering, $e^+e^- \to e^+e^-$ [9] which constrains the $H^{\pm\pm}$ boson's Yukawa couplings h_{ee} to electrons.

The DØ and CDF Collaborations at the Tevatron Collider set limits on the mass of the $H^{\pm\pm}$ in the range $M(H_L^{\pm\pm}) > 112 - 150$ GeV, assuming 100% decays into $\mu\mu$, ee, $e\tau$, and $\mu\tau$ final states [11, 12, 13, 14].

3. – The DØ Detector

The DØ detector [15] is a general purpose detector containing tracking detectors, calorimeters and a muon spectrometer. The tracking detector consists of a silicon microstrip detector and a scintillating fiber tracker which are used to reconstruct charged particle tracks within a 2 T solenoid. The calorimeter is uranium and liquid-argon based and used to measure particle energies. The selected events are required to pass triggers that select at least one muon candidate, which are identified by requiring both tracks in the central tracker and hits in the muon spectrometer.

All background and signal processes are simulated using Monte Carlo (MC) event generators, except the multijet background, which is determined from data. The W+jet, $Z/\gamma^* \to \ell^+\ell^-$, and $t\bar{t}$ processes are generated using ALPGEN [16] with showering and

hadronization provided by PYTHIA [17]. Diboson production (WW, WZ, and ZZ) and signal events are simulated using PYTHIA. The τ lepton decays are simulated with TAUOLA [18], which includes a full treatment of the tau polarization. The signal and diboson processes are normalized to next-to-leading order (NLO) quantum chromodynamics calculations of their cross sections. Next-to-NLO calculations are used for all other processes.

The generated MC samples are processed through a GEANT [19] simulation of the detector and are overlaid with data from random beam crossings which account for the detector noise and additional $p\overline{p}$ interactions in the analyzed data. Efficiency corrections are applied to the simulated distributions, for the trigger efficiency in data as function of the instantaneous luminosity. They are also applied for the differences between data and simulation in the reconstruction efficiencies and in the distribution of the longitudinal coordinate of the interaction point along the beam direction.

At DØ tau leptons are categorized into three types depending on their decays and hence their signature in the detector. Type-1 tau lepton candidates consist of a calorimeter cluster, with one associated track and no subcluster in the EM section of the calorimeter. This signature corresponds mainly to $\tau^{\pm} \to \pi^{\pm}\nu$ decays. For type-2 tau lepton candidates, an energy deposit in the EM calorimeter is required in addition to the type-1 signature, as expected for $\tau^{\pm} \to \pi^{\pm}\pi^0\nu$ decays. For type-3 tau lepton candidates, an energy deposit in the EM calorimeter and the more than one reconstructed track is required, in addition to the type-2 requirements. This corresponds mainly to the decays $\tau^{\pm} \to \pi^{\pm}\pi^{\pm}\pi^{\mp}(\pi^0)\nu$ (3-prong).

A neural network, with an output variable NN_τ designed to discriminate τ_h from jets, is trained for each tau type. The input variables are based on jet isolation variables and on the spatial distribution of showers. A requirement of $NN_\tau > 0.75$ [20] for all tau types greatly reduces the jet background significantly [5].

4. – Event Selection

The $H^{\pm\pm}$ analysis [5] requires events with at least one isolated muon and at least two τ_h candidates, where τ_h indicates a hadronically decaying tau lepton. The τ_h are restricted to type-1 or type-2 to reduce the contamination from jets misidentified as hadronically decaying tau leptons.

Each event must have a reconstructed $p\overline{p}$ interaction vertex with a longitudinal component located within 60 cm of the nominal center of the detector. The longitudinal coordinate $z_{\rm dca}$ of the distance of closest approach for each track is measured with respect to the nominal center of the detector. The differences between $z_{\rm dca}$ of the highest-p_T muon and the two highest-p_T τ_h (labeled τ_1 and τ_2), must be less than 2 cm. The pseudorapidity [21] of the selected muons, τ_1, and τ_2 must be $|\eta^{\mu}| < 1.6$ and $|\eta^{\tau_{1,2}}| < 1.5$, respectively, and for additional τ_h candidates we require $|\eta^{\tau}| < 2$. The transverse momenta must be $p_T^{\mu} > 15$ GeV and $p_T^{\tau_{1,2}} > 12.5$ GeV. All selected τ_h candidates and muons are required to be separated by $\Delta\mathcal{R}_{\mu\tau} > 0.5$, where $\Delta\mathcal{R} = \sqrt{(\Delta\phi)^2 + (\Delta\eta)^2}$ and ϕ is the azimuthal angle, and the two leading τ_h must be separated by $\Delta\mathcal{R}_{\tau_1\tau_2} > 0.7$. The sum of the charges of the highest-p_T muon, τ_1, and τ_2 is required to be $Q = \sum_{i=\mu,\tau_1,\tau_2} q_i = \pm 1$ as expected for signal events. After all selections, the main background is from diboson production and $Z \to \tau^+\tau^-$, where an additional jet mimics a lepton.

The multijet background contribution is estimated from data using three independent data samples and identical selections, except with the NN_τ requirements reversed, by requiring that either one or both τ_h candidates have $NN_\tau < 0.75$. The expected

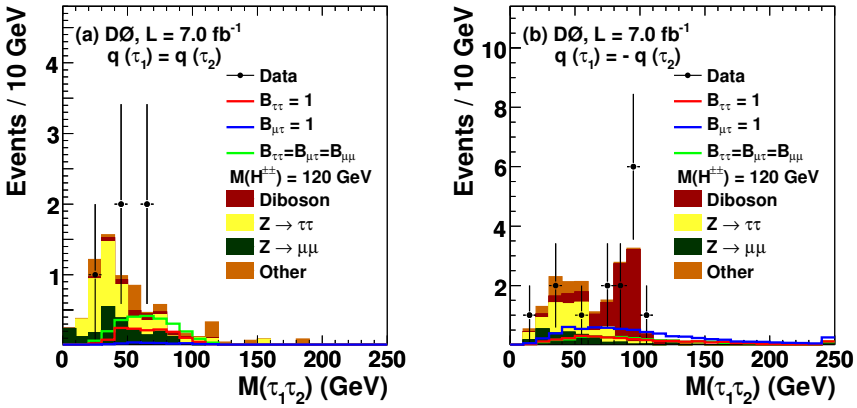

Fig. 1. – $M(\tau_1, \tau_2)$ distribution for the (a) $q_{\tau_1} = q_{\tau_2}$ and (b) $q_{\tau_1} = -q_{\tau_2}$ samples after all selections [5]. The data are compared to the sum of the expected background and to simulations of a $H_L^{\pm\pm}H_L^{\pm\pm}$ signal for $M(H^{\pm\pm}) = 120$ GeV and $\mathcal{B}(H_L^{\pm\pm} \to \tau^\pm\tau^\pm) = 1$, $\mathcal{B}(H_L^{\pm\pm} \to \mu^\pm\tau^\pm) = 1$, and $\mathcal{B}(H_L^{\pm\pm} \to \tau^\pm\tau^\pm) = \mathcal{B}(H_L^{\pm\pm} \to \mu^\pm\mu^\pm) = \mathcal{B}(H_L^{\pm\pm} \to \mu^\pm\tau^\pm) = 1/3$, normalized using the NLO calculation of the cross section. "Other" background comprises W+jet, $Z/\gamma^* \to e^+e^-$, and $t\bar{t}$ processes. All entries exceeding the range of the histogram are added to the last bin.

background simulated as described in Section 3 is subtracted before the samples are used to determine the differential distributions and normalization of the multijet background in the signal region. The total rate of expected multijet background events following all selections is negligible ($< 3\%$ of the total background).

The selected data, after all requirements are applied, are separated into four non-overlapping samples. As defined by the charges of the muon (q_μ) and the τ_h candidates (q_τ) and the number of muons (N_μ) and τ_h (N_τ) in the event. Two samples are defined where $N_\mu = 1$ and $N_\tau = 2$, and are further subdivided into the cases where both tau leptons have the same charge, $q_{\tau_1} = q_{\tau_2}$, and events with τ_1 and τ_2 of opposite charge, i.e., $q_{\tau_1} = -q_{\tau_2}$, which implies that one of the τ leptons and the muon have the same charge. This separates the cases where the $H^{\pm\pm}$ decays into two tau leptons, from when it decays into a tau lepton and a muon. The third sample is defined by $N_\tau = 3$ and the fourth sample by $N_\mu = 2$, without any additional requirements on the charges.

Figs. 1(a) and (b) show the distributions of the invariant mass of the two leading tau candidates, $M(\tau_1, \tau_2)$, for the like and opposite-charge samples. The samples have different fractions of signal and background events the like-charge sample being dominated by background from Z+jets decays and the opposite-charge sample by background from diboson production. The diboson background has a significant contribution from $WZ \to \mu\nu e^+e^-$ events where the electrons are misidentified as tau leptons [5]. The different background compositions in the separate samples increases the sensitivity to the signal. The expected number of background and signal events for the four samples and the observed numbers of events in data are shown in Table I with the statistical uncertainties of the MC samples and systematic uncertainties added in quadrature.

As the data are described well by the background prediction, limits are set on the $H^{++}H^{--}$ production cross section using a modified frequentist approach [22]. A log-likelihood ratio (LLR) test statistic is formed using the Poisson probabilities for estimated

TABLE I. – *Numbers of events in data, predicted background, and expected signal for* $M(H_L^{\pm\pm}) = 120$ *GeV, assuming the NLO calculation of the signal cross section for* $\mathcal{B}(H_L^{\pm\pm} \to \tau^\pm\tau^\pm) = 1$, $\mathcal{B}(H_L^{\pm\pm} \to \mu^\pm\tau^\pm) = 1$, *and* $\mathcal{B}(H_L^{\pm\pm} \to \tau^\pm\tau^\pm) = \mathcal{B}(H_L^{\pm\pm} \to \mu^\pm\mu^\pm) = \mathcal{B}(H_L^{\pm\pm} \to \mu^\pm\tau^\pm) = 1/3$. *The numbers are shown for the four samples separately, together with their total uncertainties.*

	All	$N_\mu = 1$, $N_\tau = 2$		$N_\mu = 1$, $N_\tau = 3$	$N_\mu = 2$, $N_\tau = 2$
		$q_{\tau_1} = q_{\tau_2}$	$q_{\tau_1} = -q_{\tau_2}$		
Signal					
$\tau^\pm\tau^\pm$	6.6 ± 0.9	1.4 ± 0.2	3.1 ± 0.4	1.6 ± 0.2	0.4 ± 0.1
$\mu^\pm\tau^\pm$	13.9 ± 1.9	0.3 ± 0.1	6.8 ± 0.9	0.4 ± 0.1	6.3 ± 0.9
Equal $\mathcal{B}$	9.5 ± 1.3	2.5 ± 0.3	3.1 ± 1.0	1.2 ± 0.2	2.6 ± 0.4
Background					
$Z \to \tau^+\tau^-$	8.2 ± 1.1	3.4 ± 0.5	4.8 ± 0.7	< 0.1	< 0.1
$Z \to \mu^+\mu^-$	5.1 ± 0.7	2.2 ± 0.3	2.5 ± 0.4	0.1 ± 0.1	0.2 ± 0.1
$Z \to e^+e^-$	0.3 ± 0.1	< 0.1	0.3 ± 0.1	< 0.1	< 0.1
W + jets	2.9 ± 0.4	1.1 ± 0.2	1.8 ± 0.3	< 0.1	< 0.1
$t\bar{t}$	0.6 ± 0.1	0.3 ± 0.1	0.3 ± 0.1	0.1 ± 0.1	< 0.1
Diboson	10.5 ± 1.7	0.5 ± 0.1	8.5 ± 1.4	0.4 ± 0.1	1.1 ± 0.2
Multijet	< 0.8	< 0.2	< 0.5	< 0.1	< 0.1
Background Sum	27.6 ± 4.9	7.5 ± 1.2	18.2 ± 3.3	0.6 ± 0.1	1.3 ± 0.2
Data	22	5	15	0	2

TABLE II. – *Expected and observed limits on* $M(H^{\pm\pm})$ *(in GeV) for left-handed and right-handed* $H^{\pm\pm}$ *bosons. Only left-handed states exist in the model that assumes equality of branching fractions into* $\tau\tau$, $\mu\tau$, *and* $\mu\mu$ *final states. We only derive limits if the expected limit on* $M(H^{\pm\pm})$ *is* ≥ 90 *GeV.*

Decay	$H_L^{\pm\pm}$		$H_R^{\pm\pm}$	
	expected	observed	expected	observed
$\mathcal{B}(H^{\pm\pm} \to \tau^\pm\tau^\pm) = 1$	116	128		
$\mathcal{B}(H^{\pm\pm} \to \mu^\pm\tau^\pm) = 1$	149	144	119	113
Equal $\mathcal{B}$ into $\tau^\pm\tau^\pm, \mu^\pm\mu^\pm, \mu^\pm\tau^\pm$	130	138		
$\mathcal{B}(H^{\pm\pm} \to \mu^\pm\mu^\pm) = 1$	180	168	154	145

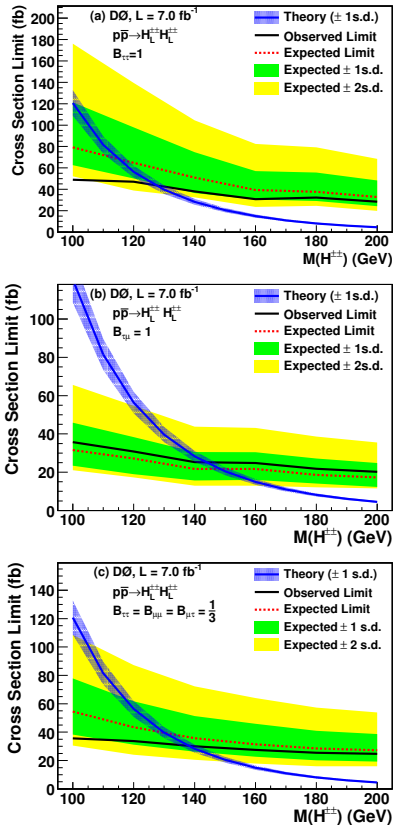

Fig. 2. – Upper limit on the $H_L^{\pm\pm}H_L^{\pm\pm}$ pair production cross section for (a) $\mathcal{B}(H_L^{\pm\pm} \to \tau^\pm\tau^\pm) = 1$, (b) $\mathcal{B}(H_L^{\pm\pm} \to \mu^\pm\tau^\pm) = 1$, and (c) $\mathcal{B}(H_L^{\pm\pm} \to \tau^\pm\tau^\pm) = \mathcal{B}(H_L^{\pm\pm} \to \mu^\pm\mu^\pm) = \mathcal{B}(H_L^{\pm\pm} \to \mu^\pm\tau^\pm) = 1/3$. The bands around the median expected limits correspond to regions of ±1 and ±2 standard deviation (s.d.), and the band around the predicted NLO cross section for signal corresponds to a theoretical uncertainty of $\pm10\%$ [5].

background yields, the signal acceptance, and the observed number of events for different $H^{\pm\pm}$ mass hypotheses. The confidence levels are derived by integrating the LLR distribution in pseudo-experiments using both the signal-plus-background (CL_{s+b}) and the background-only hypotheses (CL_b). The excluded production cross section is taken to be the cross section for which the confidence level for signal, $CL_s = CL_{s+b}/CL_b$, equals 0.05. The $M(\tau_1, \tau_2)$ distribution was used to discriminate signal from background [5].

5. – Systematic uncertainties

Systematic uncertainties on both background and signal, including their correlations, are taken into account [5]. The theoretical uncertainty on background cross sections for $Z/\gamma^* \to \ell^+\ell^-$, W+jets, $t\bar{t}$, and diboson production varies between $6\% - 10\%$. The uncertainty on the measured integrated luminosity is taken to be 6.1% [23]. The systematic uncertainty on muon identification is 2.9% per muon and the uncertainty on the identi-

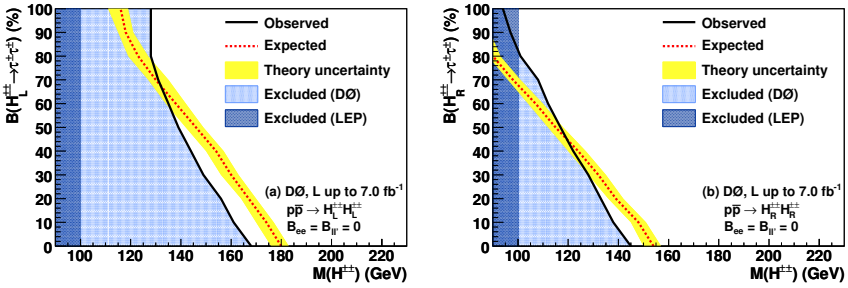

Fig. 3. – Expected and observed exclusion region at the 95% C.L. in the plane of $\mathcal{B}(H^{\pm\pm} \to \tau^{\pm}\tau^{\pm})$ versus $M(H^{\pm\pm})$, assuming $\mathcal{B}(H^{\pm\pm} \to \tau^{\pm}\tau^{\pm}) + \mathcal{B}(H^{\pm\pm} \to \mu^{\pm}\mu^{\pm}) = 1$, for (a) left-handed and (b) right-handed $H^{\pm\pm}$ bosons. The band around the expected limit represents the uncertainty on the NLO calculation of the cross section for signal [5].

fication of τ_h, including the uncertainty from applying a neural network to discriminate τ_h from jets, is 4% for each type-1 and 7% for each type-2 τ_h candidate. The trigger efficiency has a systematic uncertainty of 5%. The uncertainty on the signal acceptance from parton distribution functions is 4%.

6. – Limits

The upper limits on the cross sections are compared to the NLO signal cross sections for $H_L^{\pm\pm}H_L^{\pm\pm}$ pair production [4] in Fig. 2, for the branching ratios (a) $\mathcal{B}(H_L^{\pm\pm} \to \tau^{\pm}\tau^{\pm}) = 1$, (b) $\mathcal{B}(H_L^{\pm\pm} \to \mu^{\pm}\tau^{\pm}) = 1$, and (c) $\mathcal{B}(H_L^{\pm\pm} \to \tau^{\pm}\tau^{\pm}) = \mathcal{B}(H_L^{\pm\pm} \to \mu^{\pm}\mu^{\pm}) = \mathcal{B}(H_L^{\pm\pm} \to \mu^{\pm}\tau^{\pm}) = 1/3$. The corresponding expected and observed limits are shown in Table II.

The $H^{\pm\pm}$ boson mass limits, assuming $\mathcal{B}(H^{\pm\pm} \to \tau^{\pm}\tau^{\pm}) + \mathcal{B}(H^{\pm\pm} \to \mu^{\pm}\mu^{\pm}) = 1$ are determined by combining signal samples generated with pure 4τ, $(2\tau/2\mu)$, and 4μ final states with fractions $\mathcal{B}^2$, $2\mathcal{B}(1-\mathcal{B})$, and $(1-\mathcal{B})^2$, respectively, where $\mathcal{B} \equiv \mathcal{B}(H^{\pm\pm} \to \tau^{\pm}\tau^{\pm})$. As this analysis did not analyze a pure muon sample, a search for $H^{++}H^{--} \to 4\mu$, performed by the DØ Collaboration with 1.1 fb^{-1} of integrated luminosity [11] is included in the limit setting to account for this contribution. The invariant mass of the two highest p_T muons, including the systematic uncertainties and their correlations is used as the final discriminant. The determined mass limits are shown in Fig. 3 for varying the branching ratio to tau leptons $\mathcal{B} = 0\% - 100\%$ in steps of 10%.

7. – Summary

In summary, BSM Higgs searches with tau leptons may be of specific interest. The first search at a hadron collider for pair production of doubly-charged Higgs bosons decaying exclusively into tau leptons has been summarized as a example of such a search. This analysis set an observed (expected) lower limit of $M(H_L^{\pm\pm}) > 128$ (116) GeV for a 100% branching fraction of $H^{\pm\pm} \to \tau^{\pm}\tau^{\pm}$, $M(H_L^{\pm\pm}) > 144$ (149) GeV for a 100% branching fraction into $\mu\tau$, and $M(H_L^{\pm\pm}) > 130$ (138) GeV for a model with equal branching ratios into $\tau\tau$, $\mu\tau$, and $\mu\mu$.

REFERENCES

[1] H.P. Nilles, Phys. Rep. **110**, 1 (1984); H.E. Haber and G.L. Kane, Phys. Rep. **117**, 75 (1985).
[2] E. Ramirez Barreto, Y.A. Coutinho, and J. Sá Borges, Phys. Rev. D **83**, 075001 (2011).
[3] M. Kadastik, M. Raidal, and L. Rebane, Phys. Rev. D **77**, 115023 (2008); A. Hektor *et al.*, Nucl. Phys. **B787**, 198 (2007).
[4] M. Mühlleitner and M. Spira, Phys. Rev. D **68**, 117701 (2003) and private communications.
[5] V. M. Abazov et al. [D0 Collaboration], Phys. Rev. Lett. **108** (2012) 021801
[6] A.G. Akeroyd and M. Aoki, Phys. Rev. D **72**, 035011 (2005).
[7] G. Abbiendi *et al.* (OPAL Collaboration), Phys. Lett. B **526**, 221 (2002); P. Achard *et al.* (L3 Collaboration), Phys. Lett. B **576**, 18 (2003); J. Abdallah *et al.* (DELPHI Collaboration), Phys. Lett. B **552**, 127 (2003).
[8] A. Aktas *et al.* (H1 Collaboration), Phys. Lett. B **638**, 432 (2006).
[9] G. Abbiendi *et al.* (OPAL Collaboration), Phys. Lett. B **577**, 93 (2003).
[10] V.M. Abazov *et al.* (D0 Collaboration), Phys. Rev. Lett. **101**, 071803 (2008).
[11] V.M. Abazov *et al.* (D0 Collaboration), Phys. Rev. Lett. **93** 141801 (2004).
[12] D. Acosta *et al.* (CDF Collaboration), Phys. Rev. Lett. **93**, 221802 (2004).
[13] T. Aaltonen *et al.* (CDF Collaboration), Phys. Rev. Lett. **101**, 121801 (2008).
[14] V.M. Abazov *et al.* (D0 Collaboration), Nucl. Instrum. Methods Phys. Res. A **565**, 463 (2006); M. Abolins *et al.*, Nucl. Instrum. Methods in Phys. Res. A **584**, 75 (2008); R. Angstadt *et al.*, Nucl. Instrum. Methods in Phys. Res. A **622**, 298 (2010).
[15] M.L. Mangano *et al.*, J. High Energy Phys. **07**, 1 (2003); we use version 2.11.
[16] T. Sjöstrand, S. Mrenna, and P. Skands, J. High Energy Phys. **05**, 026 (2006); we use version 6.323.
[17] Z. Waş, Nucl. Phys. **B** Proc. Suppl. **98**, 96 (2001); we use version 2.5.04.
[18] R. Brun and F. Carminati, CERN Program Library Long Writeup W5013, 1993.
[19] V.M. Abazov *et al.* (D0 Collaboration), Phys. Rev. D **71**, 072004 (2005); erratum-ibid. D **77**, 039901 (2008).
[20] The pseudorapidity is defined as $\eta = -\ln[\tan(\theta/2)]$, where θ is the polar angle with respect to the proton beam direction.
[21] W. Fisher, FERMILAB-TM-2386-E (2006).
[22] T. Andeen *et al.*, FERMILAB-TM-2365 (2007).